



ELSEVIER

Contents lists available at ScienceDirect

Electrochimica Acta

journal homepage: www.elsevier.com/locate/electacta

Scratching the electrode surface: Insights into a high-voltage pulsed-field application from *in vitro* & *in silico* studies in indifferent fluid



Samo Mahnič-Kalamiza, Damijan Miklavčič*

Faculty of Electrical Engineering, University of Ljubljana, Tržaška c. 25, SI-1000 Ljubljana, Slovenia

ARTICLE INFO

Article history:

Received 25 June 2020

Revised 15 September 2020

Accepted 15 September 2020

Available online 12 October 2020

Keywords:

Electroporation

Electrochemistry

Electrode-electrolyte interaction

Electrical Impedance Spectroscopy

Electrode oxidation

Multiphysics modelling

ABSTRACT

Electroporation is employed ever more frequently and broadly to deliver energy to tissues and liquid media in various applications, thus answering questions on the associated electrochemistry and electrode material alteration is becoming important. The aim of the present study is firstly to introduce and elucidate the basic relations between voltage, current, electrical impedance, and heat generation in the medium, and secondly, to characterize electrode material alteration due to pulse delivery, both by performing an *in vitro* and an *in-silico* study. Saline was used as a(n) (over)simplified model medium representing biological tissue, and exposed to high-amplitude, high-current electroporation pulses of varying duration, polarity, and pulse repetition rate. The controlled experiment was conducted by using seven different electrode metals of high purity, delivering pulses using three different protocols, and concurrently or sequentially measuring as many physical properties as available (electric current, voltage, electrode-electrolyte impedance, temperature). The intent is to present a multi-physics approach to what is occurring during procedures such as *in vivo* electrochemotherapy, gene delivery and *in vitro* gene transfection, intracardiac irreversible electroporation/pulsed-field ablation, or indeed electroporation in liquid food products such as juice. Modelling is also used to see whether it is possible to detect, via electrical measurements, any alterations in medium properties (e.g. composition) due to electrochemical effects, and if any such effects can be decoupled from the ohmic and thermal effects. Water electrolysis was observed indirectly (gas production), but not detected by electrical measurements during pulse application. Reactions at the electrodes alter the electrode electrical properties depending on the electrode material as expected, which might be important especially in applications where the same electrodes are used for delivery of electroporation pulses and also for sensing small electrical signals such as ECG for example. The demonstrated approach using saline as a model medium allows for rapid validation, and can more easily be developed further, as compared to experiments with more complex electrode materials (e.g. alloys), media (e.g. fluids, growth media, biological cell suspensions), or tissues.

© 2020 The Author(s). Published by Elsevier Ltd.

This is an open access article under the CC BY-NC-ND license (<http://creativecommons.org/licenses/by-nc-nd/4.0/>)

1. Introduction

Electroporation is a phenomenon of increased electrical conductivity and permeability to mass transfer of the biological cell membrane. It occurs if a sufficiently large gradient of the electric field across the membrane is established [1,2]. Parameters of the pulse protocols (amplitude, duration, electrode geometry, etc.) for delivering the required energy to target suspension of cells or tissue are extensively researched, and used in many applications [3–6]. One

of the aspects that remains poorly investigated is however general electrochemistry. Hereby we mean an ensemble of products and consequences of Faradaic reactions at the electrode-electrolyte interface, facilitated by the electric current flowing through an electrolyte. This process is inseparably associated with delivering high-voltage pulses between an electrode pair in a conductive medium [7].

Development of electroporation applications in the food processing industry sparked an interest in associated electrochemical reactions, leading to several studies on the subject [8–15]. Electrochemical reactions in the food industry are important to understand and control due to food safety, quality (sensory percep-

* Corresponding author.

E-mail address: damijan.miklavcic@fe.uni-lj.si (D. Miklavčič).

tion), and from the technological perspective due to electrode fouling [8,9,14]. Safety is also related to the nature of electrode corrosion causing ion release, and the relative toxicity of the released metal ions that can find their way into food. However, on the grounds that exposure time of the food product to the treatment and retention time in treatment chamber are rather short, the impact of electrochemical reaction by-products to food safety appears not to have been under close scrutiny. The lack of interest can also be attributed to adoption of corrosion-resistant materials for manufacturing electrodes, such as titanium, which is a recommended metal to be used in pulsed electric field delivery systems [16]. On the other hand, there is a strong resurgence of interest in electroporation as a tissue ablation treatment, and high standards and regulations require of new treatments that their safety and efficacy be rigorously and repeatedly demonstrated by their proponents. Among the biomedical applications, it is possible to identify at least four main areas of focus: gene therapy including DNA vaccination by means of gene electrotransfer (GET) [17], electrochemotherapy (ECT) [18], irreversible electroporation (IRE) for cancer treatment [19], and cardiac ablation for treatment of atrial fibrillation [20–23].

Irreversible electroporation as a means of ablating tissue in treating atrial fibrillation is in preclinical steps with regards to interventional cardiac electrophysiology, with proven efficacy of the technique by preclinical studies [21]. Over the more conventional thermal/radiofrequency or cryoablation techniques, electroporation offers several benefits, e.g. good tissue specificity, induction of apoptosis in tissue rather than necrosis, and greater safety for adjacent structures [22,24,25]. Much the same as with thermal-based techniques for cardiac ablation, there are limitations to irreversible electroporation in its use for cardiac ablation. For example, it has previously been conjectured that in order to achieve successful long-lasting treatment effects, the electrodes need to be in good contact with tissue [26]. Recent numerical simulations indicate that proximity of the electrode to target tissue rather than direct contact is sufficient for successful ablation [27]. Irrespective of this, the contact area and quality will also affect thermal relations in treated tissue and surrounding blood, which can affect formation of coagula (denatured blood proteins) on the electrodes for high electrode temperatures [28]. Moreover, if the applied pulses have a significant DC component to them or their individual phase duration is too large, water electrolysis will lead to release of gases and formation/coalescence of bubbles. Having entered the blood stream, bubbles may cause damage, such as an embolism [29–34]. Good characterization of the phenomenon of water electrolysis and its consequences inside a beating heart is therefore of great importance for ensuring safety of the technique.

One direction in literature dealing with electrochemistry at the electrodes in the liquid medium during electroporation [7,11,13] is treating the subject as if grounded in the theory of the low-voltage electrolytic and/or galvanic cell. These cells – for reasons of practical importance and industrial interest – have been thoroughly investigated (as e.g. in the field of electroplating [35]). These traditional electrolytic/galvanic cells significantly and importantly differ in a number of aspects from the electroporation electrolytic-type cell formed by the anode(s), cathode(s), and the cell suspension or tissue. The first aspect is the difference in frequency content; while DC fields and currents are used in industrial processes such as galvanization, in electroporation, short rectangular pulses (monophasic or biphasic) are commonly delivered that are of either low, medium, or high frequency content. The frequency spectra of voltage/current for typical electroporation protocols show significant energy at higher frequencies (refer to Materials & Methods and Fig. 2b). Secondly, voltage amplitude of electroporation pulses is several orders of magnitude greater than found in industrial applications such as e.g. batteries or hydrogen fuel cells. Field

strengths can reach MV/m and the associated electric current can reach tens or even hundreds of amperes. Albeit the energy is delivered on a very short timescale [36], the amount of energy is still considerable. This places us into the poorly chartered territory of AC, high-voltage electric field electrochemistry, which we argue is different from the more familiar low-amplitude DC electrochemistry. Field strengths of 1 MV/m (in bulk electrolyte, higher fields can be reached in electric double layers at electrode surfaces) are two to three orders of magnitude shy of non-linear, non-ohmic field effects such as the Wien effect or the dissociation field effect [37]. That is not to say that a linear relationship between the voltage and the resulting current is to be automatically presupposed. We can state with certitude that a linear relationship will not be observed in biological cell suspensions or tissues for known and studied reasons [38–40]. However, by simplifying (reducing) complex biological material to the simplest electrolyte (pure saline), we have a chance to study the basics of electrochemistry using the simplest possible model of biological cell/tissue medium.

One of the principal tasks of the present study is to evaluate the (non)linearity of the voltage-current relationship, for which – if observed – we would be prepared to offer a few possible explanations. Electrode voltage and current densities at the electrode surface drive Faradaic reactions of water electrolysis (water dissociating to hydrogen protons and hydroxide ions), metal corrosion (metal ions release from the electrode), and electrode oxidation. These processes can affect the delivery of subsequent pulses by changing not only the chemical composition (and electro-/physicochemical properties in turn!) of the solution, but also the chemical composition and properties of the electrode surface (see Fig. 1). Perhaps more importantly, *in vivo* applications, electrodes delivering the treatment can also be used for sensing, i.e. for diagnostics purposes or synchronization with normal physiological functions. For example, in electroporation for treating atrial fibrillation, the electrodes used for treatment may also be used for obtaining intracardial electrograms [22]. Changing properties of electrodes is undesirable, as it can lead to amplification or attenuation of the signal received from the electrodes during sensing. It is also conceivable that thermal sensors (e.g. thermocouples) be integrated into the pulse-delivering electrodes to monitor the temperature at the electrode-tissue or electrode-blood interface. This is important for minimizing risk of electrode fouling by protein deposits and formation of potentially dangerous coagula that could embolize and enter the blood stream. We have set out to evaluate how important electrode material alteration is by measuring the pre- to post-pulse impedance of the electrode-electrolyte system. We compare impedance measured for a repeatedly used electrode pair with impedance of a “new” (i.e. refurbished surface) electrode pair during consecutive repeats. The findings are relevant not only in the domain of biomedicine, where repeated reuse of electrodes in labs and veterinary practices can be problematic, but also in food engineering [41]. Devices are already reaching the market using electroporation in combination with ohmic heating to process food, intended for both professional and domestic use [42].

The other direction examining electrochemistry of electroporation focuses on the effects of products of water electrolysis, i.e. H^+ and OH^- ions, causing pH changes – an acidic front at the anode, and an alkaline front at the cathode side [43]. These pH changes can be so intense as to be damaging to the cells (pro- and eukaryotic) and tissues, to an extent that allows for a treatment called “electrolytic ablation”. In electrolytic ablation, the strong acidic and alkaline front advancing through the tissue during application of electric current are used to ablate the tissue [44–47]. Strongly acidic or alkaline medium can also result in transient or permanent changes in molecules, e.g. it can cause DNA denaturation and permanent damage through depurination and strand breakage [48–50].

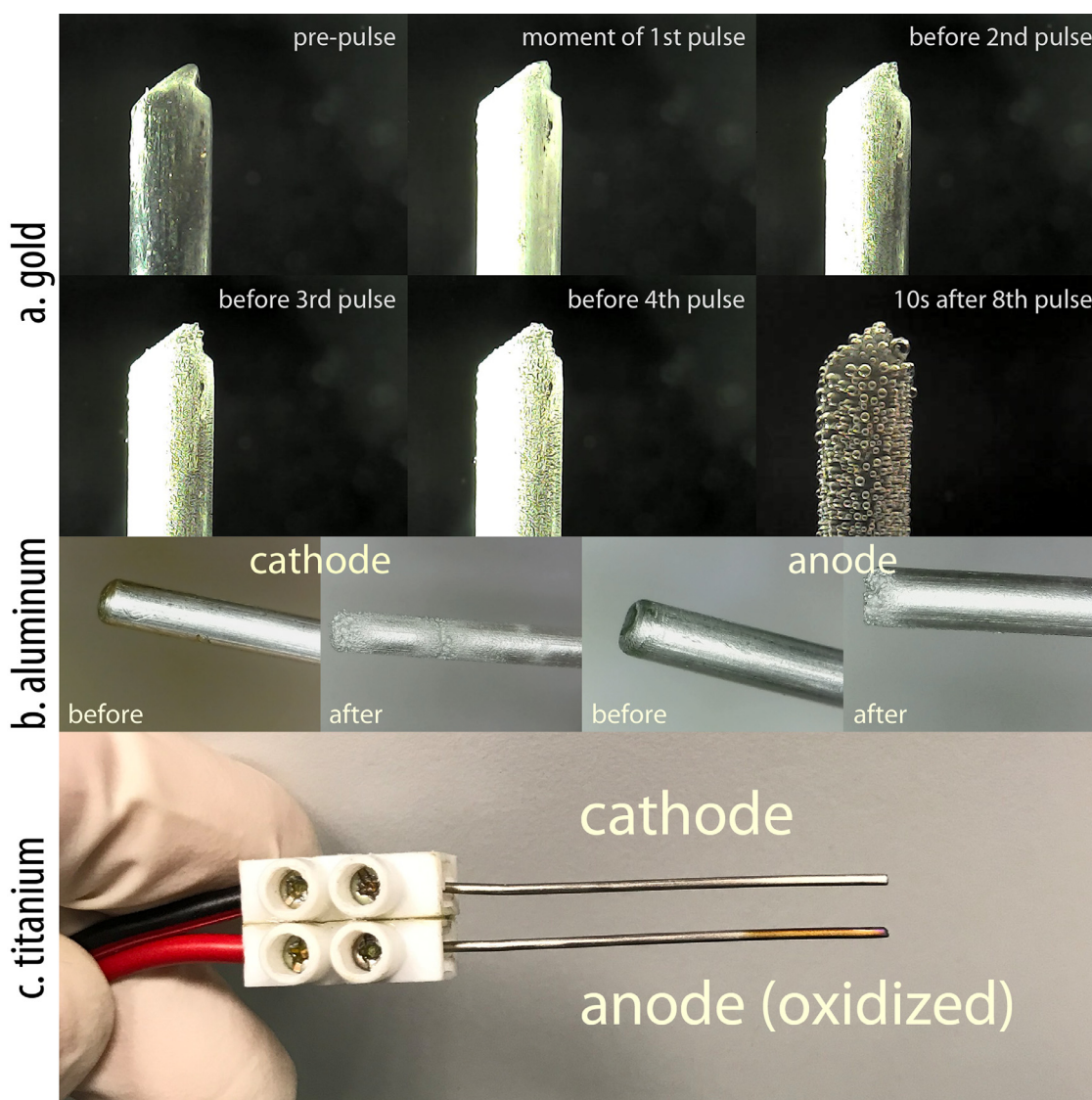


Fig. 1. Photos demonstrating macroscopically observable changes and phenomena evidencing electrochemistry at the electrodes. Experiments for preparing all presented photos were performed in 0.9% saline. (a) hydrogen gas production by water electrolysis at the cathode and subsequent bubble formation/coalescence (pure gold electrode) during application of eight 100 μ s monophasic pulses – the sequence of images demonstrates appearance of many smaller hydrogen gas bubbles at the moment of pulse delivery, causing the light illuminating the electrode to refract on the bubbles, resulting in a “glow” effect, and coalescence of smaller bubbles to form larger ones, (b) metal corrosion (aluminum cathode and anode, before and after extensive use in experiments), the strong etching of the tip is evident – a phenomenon particularly characteristic of aluminum electrodes, and (c) oxidized anode (pure titanium) tip – the discolored part of the anode was submerged in saline during pulse delivery. Images of electrodes before and after the ten seconds after the last pulse delivery are omitted from presentation, see video in the supplementary materials for a complete chronological sequence.

Another important aspect when analyzing the voltage-current relationship in an electrolyte solution is the effect of Joule heating [38,51]. Electrical conductivity of saline (solution of NaCl in water) substantially increases with temperature (dependence is stronger than that of pure water [52,53]), thus increasing the current at a given voltage. The reason is that current, Joule heating, and conductivity are interlocked in a positive feedback loop (a case of possible thermal runaway). Performing any sort of precise conductivity measurements therefore requires careful control of the temperature. A model simulation was set up to delineate the impact of any electrochemistry to saline conductance or impedance from the contribution of heating. The simulation enables us to theoretically estimate how conductivity would behave, were it only for the effect of increased temperature. The 3D dynamical model is being fed with the applied pulses recorded during the *in vitro* experimental run. The simulation couples the physics of electric currents, Joule heating, and heat transfer in liquids in order to simulate the

resulting current, which is compared to experimentally recorded data.

To demonstrate some of the electrochemical phenomena at the macro scale observed during experiments, we present Fig. 1, which shows some of the effects observed at or on the electrodes. Electrode corrosion is a known and ubiquitous problem, mitigated by frequent changes of electrodes and/or using less reactive (noble) metals and materials. Another potential issue is the formation of oxygen, chlorine, and hydrogen bubbles. Regardless of whether the bubbles are thermally or electrochemically produced, their formation and circulation along the blood stream pose challenges due to their potentially pathological effects to tissues such as brain and/or renal microinfarctions, etc. [29–34]. For an ultrasound image of hyperechoic areas in liver during electrochemotherapy attributable to bubbles forming and migrating with blood flow, see figures in [54]. Video of hydrogen gas bubbles forming at the cathode in 0.9% saline can also be found among the supplement-

tary materials to this paper (selected frames are presented as part of Fig. 1).

Fig. 1 demonstrates why further studies of electrochemistry in electroporation are necessary, and why, with the work presented herein, we have quite literally just barely scratched the surface of the subject in hand.

2. Materials and methods

2.1. in vitro experiments

We used 0.9% saline solution, in present time commonly referred to as normal or physiological saline. We refer to it in the title of this paper under its original name “indifferent fluid” for reasons explained in [55], and in continuation simply as saline for brevity. Saline is a commonly used model of blood plasma or interstitial fluid, kept simple enough for permitting theoretical analysis of results. The saline was prepared as a 0.9% (w/v) NaCl in water solution using water for ultratrace analysis (cat. no. 14211, Sigma-Aldrich) and 99.999% pure NaCl (cat. no. 204439, Sigma-Aldrich, USA). To confirm whether thusly prepared pure saline is a good approximation of a medium normally used for cell electroporation *in vitro* in terms of conductivity, we also performed a limited set of voltage and current measurements using the cell growth medium Nutrient Mixture F-12 Ham (cat. no. N6658, Sigma-Aldrich, USA).

Electric pulses using three different electroporation protocols were applied to the saline using needle electrodes made of seven different metals of high purity and/or metal alloys of known composition. Voltage and current were recorded in sequential capture (segmented memory) mode with a DSO (digital storage oscilloscope) LeCroy HDO6104A-MS (Teledyne LeCroy, USA), while solution temperature was continuously recorded during pulse delivery. For temperature sensor location, refer to Fig. 8a. Impedance before and after pulse delivery was measured over a wide spectrum of frequencies with a Keysight E4980A (Keysight Technologies, USA) impedance analyzer utilizing the two-electrode method. The authors are aware of and fully acknowledge the limitations and disadvantages of using a two-electrode method for impedance measurements in lieu of the three- or four-electrode approach, however, as demonstrated in continuation (see Fig. 10 discussion), this choice was intentional.

The three electroporation protocols were chosen such that the ensemble consisted of one well-established protocol (in fields of ECT and IRE) and two protocols of short biphasic pulses (see Fig. 2a). The use of biphasic pulses has seen a strong resurgence recently in electroporation research due to several alleged benefits over longer, monophasic pulses, namely: *i*) more tolerable and less intense muscle contractions due to lower degrees of indirect or direct muscle stimulation [56–58], and *ii*) a better charge balance and reduced post-pulse polarization. Shorter biphasic pulses are associated with less pronounced electrochemical phenomena at the electrodes, are more likely to have a locally neutral pH impact (alternating anode-cathode), and less intensively promote oxidation/metal erosion. In aid of interpretation of the following protocols description, bold letters in the text correspond to designations in Fig. 2a. Protocol 4-5-4-800: positive phase pulse of 4 μ s, interphase delay of 5 μ s, followed by a negative phase pulse of 4 μ s (this 4-5-4 sequence forms one biphasic pulse \mathbf{p}_i), followed by an 800 μ s inter-pulse delay, a single such group (\mathbf{G}_1) of 100 (\mathbf{p}_1 to \mathbf{p}_{100}) biphasic pulses was delivered in a single train (\mathbf{T}_1); and Protocol 1-1-1-1000: 1 μ s positive phase pulse width, 1 μ s interphase delay, followed by a negative phase pulse of 1 μ s width, with a 1000 μ s (1 ms) inter-pulse delay, 400 such biphasic pulses (\mathbf{p}_1 to \mathbf{p}_{400}) were delivered in a single group (\mathbf{G}_1) of a single train (\mathbf{T}_1).

For the monophasic pulse protocol, we chose the standard electrochemotherapy protocol [59] of 8 pulses (\mathbf{p}_1 to \mathbf{p}_8), all 100 μ s

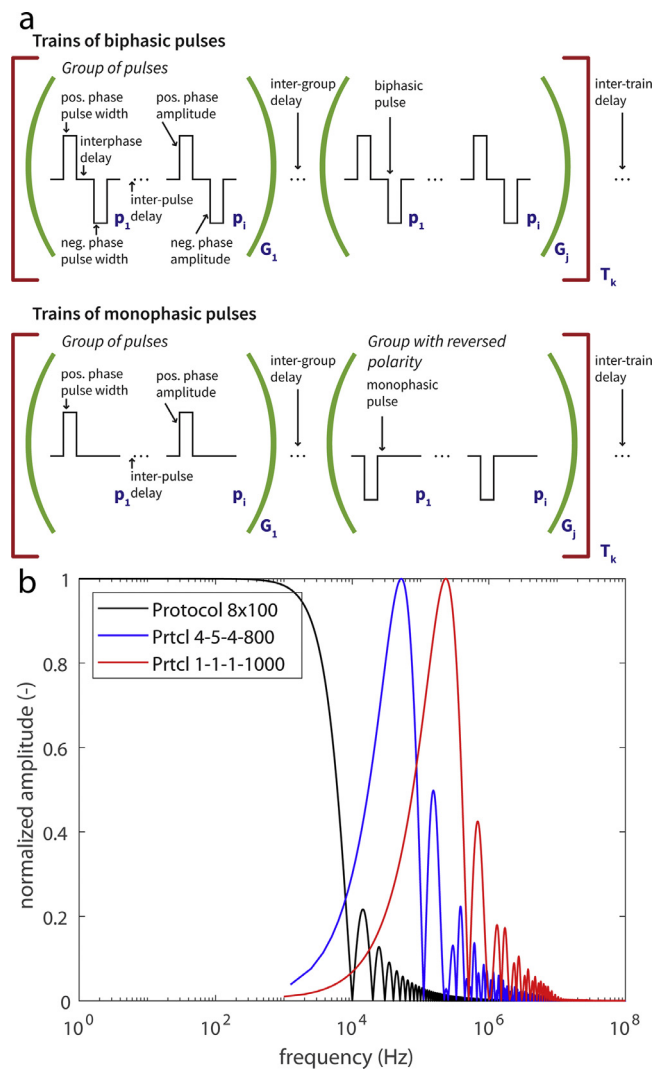


Fig. 2. Pulses used in experiments and simulations; (a) generalized schematic representations of pulse protocols consisting of biphasic (upper subfigure) or monophasic (lower subfigure) pulses as visual aids in understanding durations of pulses and delays; (b) amplitude-normalized Fourier single-sided spectra of the pulse protocols used in the study. The bulk of the energy of the monophasic 100 μ s pulses is in the DC to about 10 kHz range, while the two biphasic pulse protocols' energy peaks are in the higher, 50–200 kHz range, and their DC component tends towards zero since they are biphasic.

Table 1

A summary presentation of the three pulse protocols used.

Parameter/Protocol	“4-5-4-800”	“1-1-1-1000”	“8 × 100”
No. of pulses delivered	100	400	8
Mono- vs. biphasic	biphasic	biphasic	monophasic
Repetition frequency* [Hz]	1230	997	3
Single phase length	4	1	n/a
Single pulse length* [μs]	13	3	100
Interphase delay [μs]	5	1	n/a
Inter-pulse delay [μs]	800	1000	999,900

* Both phases together with the inter-phase delay (where applicable) form a single pulse.

long [23], monophasic, with 1 Hz repetition frequency (inter-pulse delay of 999.9 ms), with no reversal in polarity. Only one group (\mathbf{G}_1) of 8 pulses in a single train (\mathbf{T}_1) was delivered. This protocol is henceforth referred to as Protocol 8 × 100. For a clearer overview of the three protocols used, protocol parameters are collected and presented in Table 1.

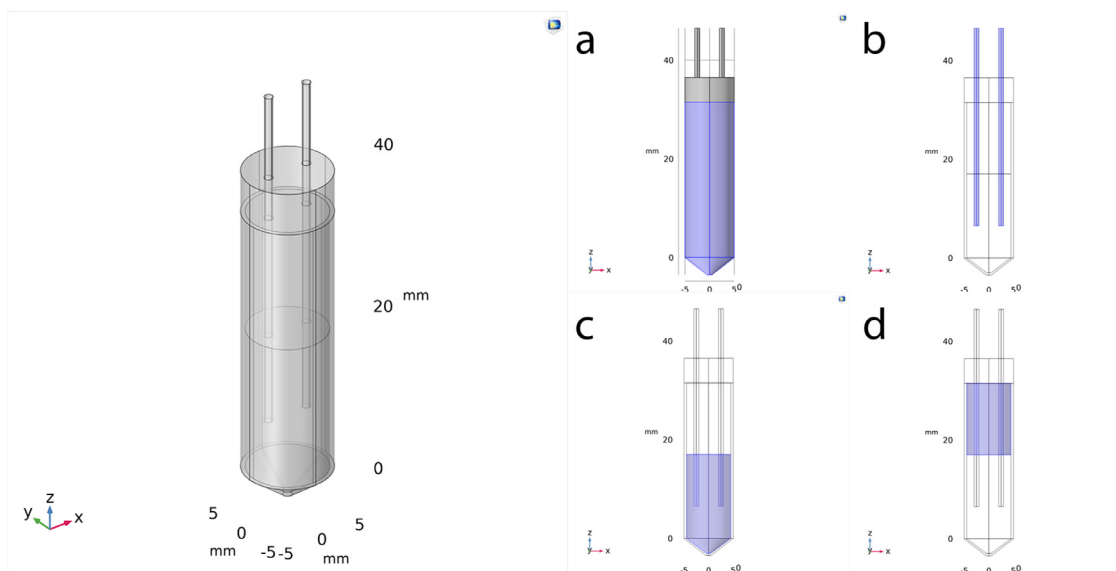


Fig. 3. Treatment chamber schematic. The 3D model as presented was drawn in COMSOL Multiphysics. Complete model on the left; (a) microcentrifuge, (b) electrodes, (c) saline, and (d) air.

Fig. 2b presents an amplitude-normalized Fourier single-sided spectrum of the three pulse protocols representing the frequency content of used signals. Notice the Protocol 8×100 amplitude spectrum differs significantly from the remaining two protocols, its amplitude extending well into the DC range of frequencies; we thus expect to see more pronounced electrochemistry effects (production of gas, change of electrode impedance, ...) with this protocol.

The pulse number for each protocol was chosen such that all three protocols would, were the voltage-current relationship and electrical conductivity completely frequency-independent, yield precisely the same energy delivered within a single train of pulses. The total pulse train duration (time during which the pulse is "ON", in food applications also termed *total treatment time*) is equilibrated across the three protocols, totaling 800 μ s. Voltage at the electrodes as set on the generator was 500 V in all cases except in the part of the study performed to establish the voltage-current relationship, where it was set at either 100, 200, 300, 400, or 500 V (see Fig. 6).

For the treatment chamber, a standard 2 mL microcentrifuge tube (ISOLAB, Germany) was used with a custom 3D-printed top through which three holes were drilled; two holes for the two electrodes, and one for the optic fiber temperature probe. The electrodes were cylindrical in shape, of 1 mm diameter, spaced 5 mm apart cylinder center-to-center. The geometry is given in Fig. 3 and can also be found among the supplementary materials. The temperature probe was inserted through the third hole in the plastic top located slightly (by 1 mm) off the hypothetical center line drawn through both the electrode holes, and equidistant to the two electrodes. The temperature was recorded using an OpSens optical thermometer PSC-D-N-N with single channel module PSR-G1-10-100ST (OpSens Solutions Inc, Canada) and an OTG-MPK5 fiber optic temperature sensor from the same manufacturer. The optic sensor used has a response time lower than 225 ms and high accuracy of ± 0.3 °C over its operating range of 20 to 45 °C. The chamber was partially filled with 1.1 mL of 0.9% saline, and electrodes were immersed into the saline such that the distance between the bottom of the electrodes and the bottom of the plastic top of the microcentrifuge was exactly 25 mm. This configuration results in 10.5 mm of each electrode being immersed in saline for a total area of 33 mm²

(i.e. the surface of the electrode immersed in saline, per one electrode).

Electrode materials were of high purity, pairs of electrodes were made from: platinum electrodes 99.99% pure Pt (cat. no. PT005155, Goodfellow Cambridge); stainless steel 304 (cat. no. FE225150, Goodfellow Cambridge) composed of 17–20% Cr, < 2% Mn, 8–11% Ni, < 800 ppm C and Fe balance; titanium was 99+% pure grade-2 titanium (Gema Fast, Netherlands); nitinol (Ni/Ti alloy) was nitinol Niti#1 (Fort Wayne Metals, Ireland) composed of 54.5 – 57.0% Ni, max. 500 ppm C, max. 500 ppm N + O, max. 50 ppm H and Ti balance; tantalum used was 99.9% pure Ta (cat. no. TA005160, Goodfellow Cambridge); gold was 99.99% pure Au (cat. no. AU005170, Goodfellow Cambridge); and the platinum-iridium alloy was 99.9+% pure Pt/Ir 90/10 (cat. no. 900817, MaTeck (Germany)).

For the purposes of producing video recordings and images of bubble release and electrode erosion as presented in Fig. 1, we used an unbranded digital microscopic camera with adjustable zoom (1x to 1000x) and focus. For the bubble release recordings, the electrodes were immersed into saline inside cell culture flasks of 25 cm² growth area (TPP, Switzerland) and video was recorded through one of the two optically transparent polystyrene sides of the vessel. Cell culture flasks were used exclusively for recording bubble release videos due to their optic properties and were not used elsewhere in this study. In all other geometrical aspects (e.g. inter-electrode distance, electrode diameter, depth of immersion into saline), the bubble release setup is identical to the setup using microcentrifuges.

The complete experimental setup can be found in Fig. 4. Additional components not previously mentioned involve a laptop computer for recording the temperature (via an Ethernet link) and impedance (via a USB link), and also controlling a custom-made relay switchbox (University of Ljubljana, Faculty of Electrical Engineering, Laboratory of Biocybernetics) that permits fast manually- or software-controlled timed switching of electrodes between the pulse generator and the impedance analyzer. The complete schematics of the circuit board of the switchbox are available among the supplementary materials. Pulse generator used was a tablet-controlled laboratory unit custom designed and built, H-bridge based digital amplifier with 1 kV MOSFETs (DE275-102N06A, IXYS, USA) [60].

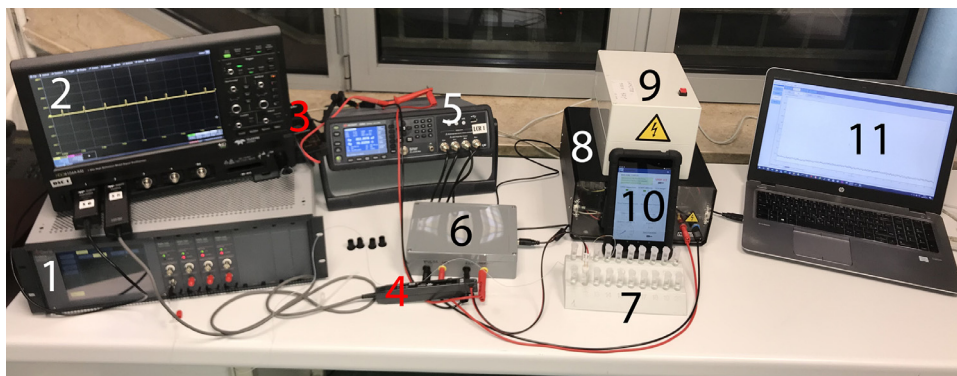


Fig. 4. The complete experimental setup. From left to right: Optical thermometer (1) and a sequencing DSO (2) with high-frequency, high-voltage (3) and high-current (4) probes, impedance analyzer (5) and computer-controlled relay switchbox (6), microcentrifuge stand (7) and pulse generator (8) with an additional externally-housed capacitor (9) and tablet control unit (10), and a laptop computer (11) for data acquisition and switching control.

2.2. In silico modelling

COMSOL Multiphysics (COMSOL AB, Sweden) was used to model the microcentrifuge and the saline with immersed electrodes to simulate the experimental setup with geometry shown in Fig. 3. The model involves Electric Currents and Heat Transfer in Liquids physics and features a time-dependent study whereby either heat transfer and electric currents are modelled concurrently (during the pulse “ON” time), or heat transfer exclusively (during the pulse “OFF” time). The Electric Currents and Heat Transfer physics are coupled via the electric current (Joule heating) and conductivity of saline; electric current through the saline as an ohmic load generates heat, which raises conductivity, which in turn augments the current. During the pulse “OFF” time, heat dissipates to an extent which is an effect particularly important for pulse protocol 8×100 . Heat transfer is included by means of the Heat Transfer in Solids and Fluids physics in COMSOL, which effectively means we are modelling conduction (w/o mixing) through a liquid and through solid electrodes. Microcentrifuge tube is considered an ideal isolator, i.e. heat conservation principle applies to the system. Heat generation due to current flow is modelled via inclusion of the Electromagnetic Heating Multiphysics module, coupling the Electric Currents physics describing the electrical relations in the system with the aforementioned Heat Transfer in Solids and Fluids physics for the thermal model.

The time-dependent electric currents model requires prescribed voltage at the electrodes as a boundary condition. We prepared a suitable experimentally recorded pulse train sample for each pulse protocol that was sampled on the DSO at high frequency, then filtered and decimated using MATLAB (Mathworks, USA), and imported into COMSOL as *interpolation functions* (in COMSOL terminology). The raw signals and their filtered counterparts are presented for a single $100 \mu\text{s}$ pulse (Protocol 8×100) in Fig. 5. Note that we neglect the effects of electrode polarization on the results of the simulation, since the voltages on the electrodes during pulses are on the order of hundreds of V, orders of magnitude above the voltage drop on the ionic double layer. The output of the simulation is the resulting current flowing between the two electrodes, obtained from the model by means of ordinary surface integration of the normal current density (designated *ec.nj* by COMSOL) along a single electrode. This resulting calculated current can then be compared against the experimentally recorded current for analysis.

Note that voltage and current pulse shapes for biphasic pulses are similar in terms of noise and transient phenomena to the Protocol 8×100 examples in Fig. 5, and so are omitted from the paper for brevity. Also note that consecutive pulses will look almost identical to the first pulse for the voltage signal, however the cur-

rent will slightly increase in amplitude due to conductivity changes brought about by Joule heating.

3. Modelling the current distribution

In order to support our modelling approach, we present a short theoretical introduction, based on COMSOL’s documentation on applicability and use of the primary, secondary, and tertiary current distributions, as available from [61,62].

The electrolyte is an ionic conductor, wherein the net current density can be described as:

$$i_l = F \sum_i z_i N_i \quad (1)$$

where i_l denotes the current density vector (A/m^2) in the electrolyte, F is the Faraday constant (C/mol), and N_i the flux of species i ($\text{mol}/(\text{m}^2 \cdot \text{s})$). The electrolyte charge number is denoted z_i . The flux of an ion in an ideal electrolyte solution can be described by the Nernst–Planck equation, which accounts for the flux of solute species by convection, migration, and diffusion, as follows in Eq. (2):

$$N_i = c_i \mathbf{u} - z_i u_{m,i} F c_i \nabla \phi_l - D_i \nabla c_i \quad (2)$$

In Eq. (2), c_i is the concentration of the ionic species i (mol/m^3), D_i is the diffusion coefficient for ion i (m^2/s), $u_{m,i}$ the mobility of ionic species i in the given electrolyte ($\text{s} \cdot \text{mol}/\text{kg}$), ϕ_l is the electrolyte potential, and \mathbf{u} the velocity vector (m/s).

Inserting the Nernst–Planck equation (Eq. (2)) back into the expression for current density (Eq. (1)), we obtain:

$$i_l = uF \sum_i z_i c_i - F^2 \nabla \phi_l \sum_i z_i^2 \frac{D_i}{RT} c_i - F \left(\nabla \sum_i z_i D_i c_i \right) \quad (3)$$

where we have also substituted the mobility for its resolved term of D_i/RT . The principal governing equation is the conservation of current, which in general must include the electrolyte current source term Q_l (A/m^3):

$$\nabla \cdot i_l = Q_l \quad (4)$$

The conservation of charge must be respected throughout, and in general it must also be conserved at the interface of the electrode and the electrolyte. Between these two domains, current is transferred either by an electrochemical reaction (i.e. electrolysis or Faradaic current), or by dynamic charging or discharging of the charged double layer of ions at the surface of the electrode, which is called capacitive or non-Faradaic current.

If we can assume that one or more of the terms in Eq. (3) are sufficiently small to be negligible, equations simplify. There are

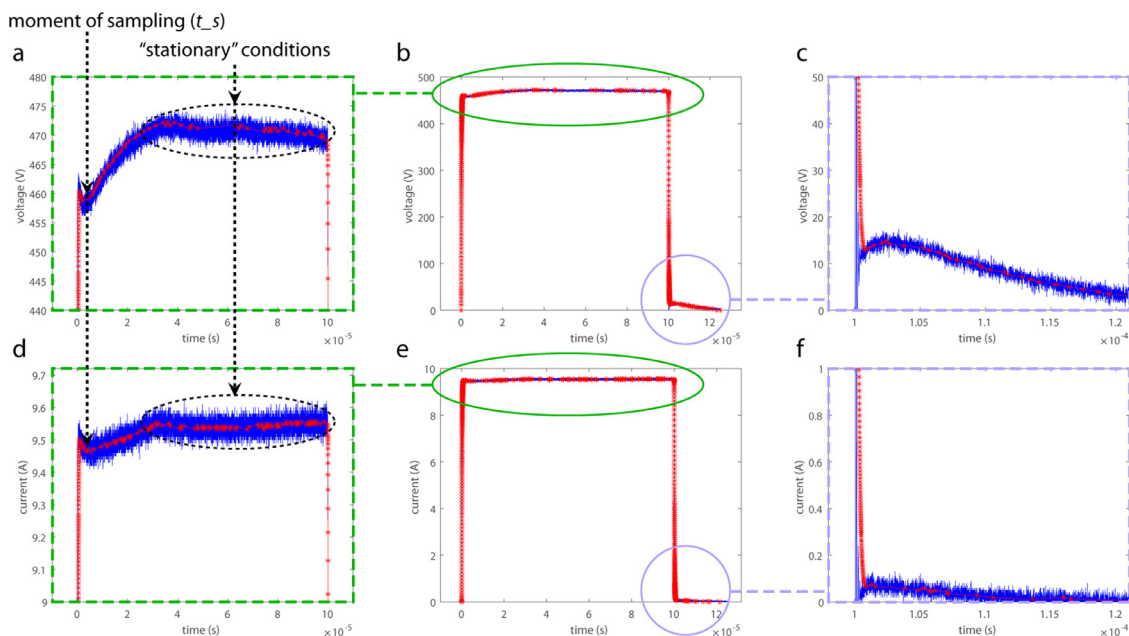


Fig. 5. Experimentally recorded pulse voltage (a-c) and current (d-e) and the corresponding filtered and decimated signals. The raw signal as captured is shown in blue, decimated signal in red. Subfigures (a) and (d) are zoomed in along the ordinate to render noise and amplitude dynamics more visible, while (c) and (f) show the pulse turn-off transitory phenomenon and the effect of filtering to its elimination before the signal is imported for use into COMSOL. Signals featured in this figure are captures of Protocol 8×100 , where only the first pulse (out of 8 in a train delivered at 1 Hz) is shown. (For interpretation of the references to colour in this figure legend, the reader is referred to the web version of this article.)

three different current distribution classes in electrochemical analysis (the primary, secondary, and tertiary current distribution), which one of them is applicable depends on assumptions. These are chosen depending on the relative influence of different contributing factors affecting the current distribution (convection vs. migration vs. diffusion) when analyzing the Nernst-Planck equation.

The primary current distribution accounts only for losses due to solution resistance, neglecting the impact of finite rate of electrode kinetics and concentration-dependent effects. The charge transfer in the electrolyte is assumed to obey Ohm's law. This supposition is based on two important assumptions: firstly, we assume electrolyte electroneutrality, i.e. $\sum_i z_i c_i = 0$; and secondly, we assume composition variations in the electrolyte to be negligible (homogeneous electrolyte). These assumptions leave us only with the middle term on the right-hand side of Eq. (3), which results in Ohm's law for electrolyte current density.

$$i_l = -F^2 \nabla \phi_l \sum_i z_i^2 \frac{D_i}{RT} c_i \quad (5)$$

Note that the assumption of electroneutrality is reasonable for an aqueous electrolyte solution, but not necessarily for biological systems where charge separation on the ion-selective membrane can occur.

For considering only the primary current distribution, another assumption must be made concerning the conditions at the electrode-electrolyte interface. If we can assume that the electrolysis reaction is fast enough, it is possible to neglect the finite rate of electrode kinetics, then the potential difference at the electrode-electrolyte interface should not significantly deviate from its equilibrium value. This means there should be an absence of an activation overpotential, and an arbitrary current density can occur anywhere along the surface of the electrodes through electrolysis. If so, then the primary current distribution only depends on the geometry of the anode and of the cathode.

If the above assumptions can be made, the electric current density is as given by Eq. (5), and the system governing equations are thus

$$\nabla \cdot (-\sigma \nabla \phi_l) = 0 \quad (6)$$

$$\sigma = F^2 \sum_i z_i^2 \frac{D_i}{RT} c_i \quad (7)$$

where σ denotes electrical conductivity (S/m).

4. Results and discussion

4.1. Pulse protocol and the voltage-current relationship

In order to determine whether electrode-saline system behaves as an ohmic load for electroporation protocols tested, we first performed a simple experiment to see if the voltage-current relationship is indeed linear, at least in the stationary state of the pulse, i.e. after the transient response of the system has passed. The same experiment was then simulated using the COMSOL model to see if it can predict the measured currents, which it successfully managed. The initial electrical conductivity of saline was obtained from tabulated data by interpolation or extrapolation, based on the given concentration of NaCl and saline temperature [53,63,64]. For analysis we took the initial current values after the transient phenomenon or "capacitive charging spike" (see Fig. 5) in current due to electrode polarization and (re)orientation of water dipoles in the saline can be considered complete, and before the onset of significant changes in conductivity due to Joule heating of the saline (refer to moment of sampling, t_s , in Fig. 5). The results are presented in Fig. 6.

As Fig. 6 clearly demonstrates there is a remarkably linear relationship between the voltage at the electrodes and the current through the electrolyte. This relationship was verified also in the growth medium (i.e. F-12 Ham – data not presented), from which we can conclude that 0.9% saline is a good model for delivering

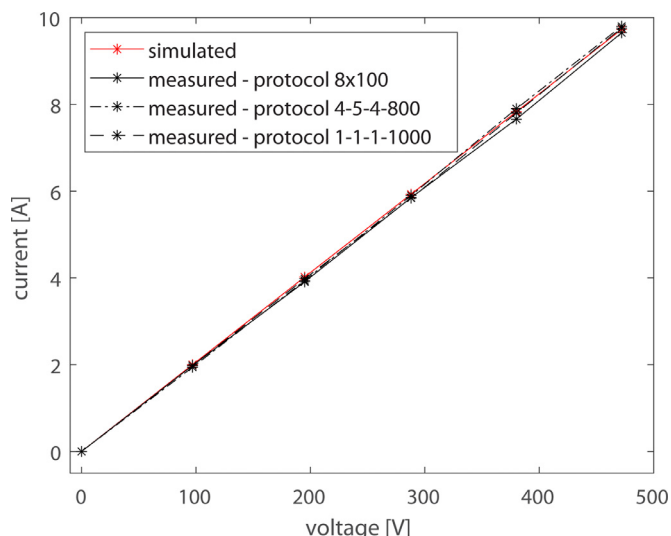


Fig. 6. The electric current as a function of voltage for the three pulse protocols at five different voltages in the range of 100 to 500 V.

pulses in the growth medium from an electric perspective. Were we to use smaller voltages (within range of mV or up to a few V), we would expect to see a nonlinear relationship, since electrode kinetics (finite rate of electrolysis), and limited diffusion rate play an important role at low voltages. This confirmation of the ohmic behavior of our electrode-electrolyte system is important as it justifies the use of the simpler Electric Currents module in COMSOL. At this point we should also demonstrate, by means of a quick calculation, that the solution composition remains largely unaffected by water electrolysis. Experimental current amplitude was just shy of 10 A. For 8 pulses of 100 μ s, this equals 0.0076 C of charge, which results in the electrolysis of about 4×10^{-8} mol water, which is less than 0.07% of the total amount of water in the microcentrifuge tube; meaning that the chemical composition of the medium remains largely unaffected by water electrolysis.

4.2. The coupled temperature-current model – effect of heating on saline conductivity

As previously mentioned, the electric current flowing through saline at a constant voltage is expected to rise due to Joule heating of the medium. Heating the medium will increase its electrical conductivity, rising the current. The 0.9% saline exhibits a dependence of the electrical conductivity on the temperature, in the range of about 2.3 to 2.5%/ $^{\circ}$ C [53,63]. The increase in current can be seen during the pulse (intra-pulse), provided the pulse is long enough to result in considerable heating of the saline. There can also be noticeable heating from one pulse to the next (inter-pulse) if the pause between pulses is sufficiently short. The intra-pulse

current augmentation due to changes in medium conductivity can be observed for the case of Protocol 8×100 , see Fig. 5; while the voltage begins to drop during the second half of the pulse, the current is still augmenting, albeit marginally. In case of a purely ohmic load, this can only be interpreted as direct consequence of increased saline conductivity. We have confirmed this by performing an EIS (electrical impedance spectroscopy) analysis of the saline over a range of temperatures and estimated conductivity from the high-frequency impedance. For further information, refer to the results comments accompanying Table 2.

Our model, provided with the voltage signal $u(t)$ at the electrodes and the conductivity as a function of temperature curve – $\sigma(T)$, simulates the electric current density distribution $\mathbf{i}(t_0)$ at the beginning of the pulse. This current results in inhomogeneous Joule heating $Q(\mathbf{i})$, and we obtain the resulting temperature distribution $T(t_0)$ within the saline. This distribution is, during the next time step (voltage remains constant or changes according to the input voltage signal $u(t)$), used to recalculate the electrical conductivity $\sigma(t_1)$ distribution according to the $\sigma(T)$ curve. This conductivity is then used to obtain the electric current density distribution $\mathbf{i}(t_1)$, and so forth until the end of the simulation. Fig. 7 illustrates this process with a current density distribution and a temperature distribution at the end of a single 100 μ s pulse. Note that the measured conductivity during the pulse is about 50 Ω , which may seem low upon first evaluation of the setup geometry. However, as the current density distribution in Fig. 7b clearly shows, current flow lines deviate in the radial direction. Current is thus dispersed over a wider area/greater volume, and the effective area for current to flow is effectively much larger than if the electrodes were parallel plates of equal dimensions as needles, and with the medium only present in between the electrodes.

Most significant weakness of the presented experimental approach stems from the method of measuring and recording temperature during pulse application, the accuracy of which is important for model validation purposes, but unfortunately the measurement exhibits strong sensitivity to sensor placement due to small chamber dimensions, comparably large size of the temperature sensor, and inhomogeneity in current and heat distributions due to use of thin needle electrodes (use of plate electrodes would have helped in this respect). It is with considerable difficulty that we can ensure the tip of the temperature sensor is placed consistently into the microcentrifuge into precisely the same point every time (relative to the electrodes). For experimentation we have endeavored to prepare and maintain the temperature sensor setup to be as stable as possible by making the plastic tops of microcentrifuge tubes thick enough, so that the opening through which the sensor is inserted also acted as a guide, stabilizing the sensor in the axes x and y (see Fig. 8) that are perpendicular to the axis of insertion (i.e. z). In the direction along the electrode insertion (z coordinate in the model, see Fig. 3), repeatability can be improved if we aim for such depth of needle electrode insertion so that the needle electrode tips are aligned with the tip of the sensor when

Table 2

Experimentally recorded relative current increase from first to last pulse vs. the corresponding current increase as predicted based on temperature increase, for all three tested pulse protocols. Gold (Au) electrodes were used for experiments to limit the effects of electrode oxidation, pitting, etc. Voltage was 500 V in all experiments used to produce the table.

	Relative measured current increase [%]	Measured temperature rise [K]	Predicted relative current increase [%]	Absolute error predicted to measured current increase [%]
Protocol 8×100	3.12	1.47	3.17	0.05
Protocol 4-5-4-800	2.97	1.40	3.02	0.05
Protocol 1-1-1-1000	4.27	1.93	4.19	-0.08

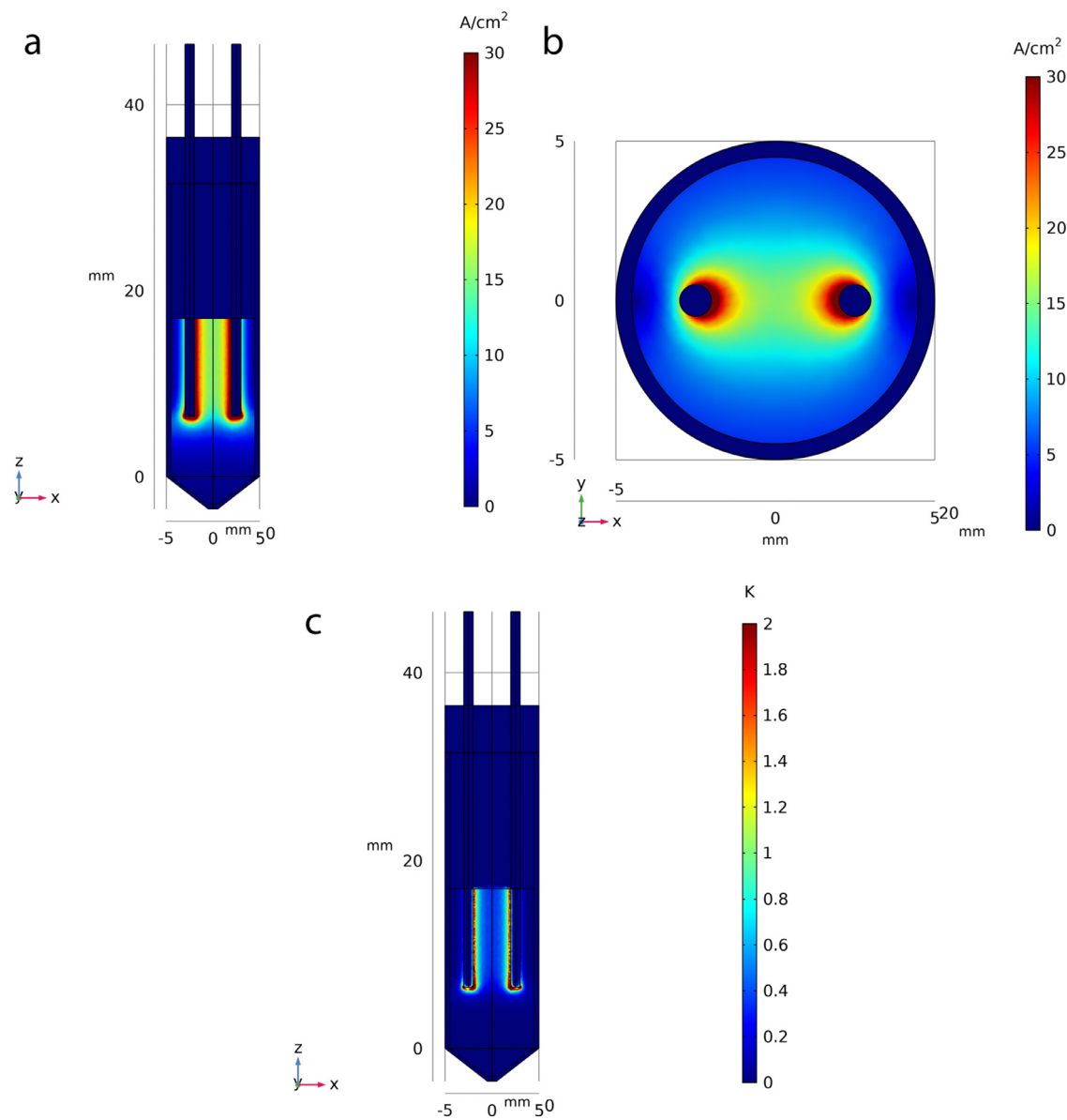


Fig. 7. Numerical simulations (COMSOL); current density distributions in two different geometrical cross-sections (a & b), and c) overtemperature (absolute minus ambient) distribution at the end of the first 100 μ s pulse (Protocol 8 \times 100). The base (ambient) temperature was 299.15 K (26 $^{\circ}$ C), which augmented locally to a maximum of 302.30 K (29.15 $^{\circ}$ C) at the hottest point close to the tip of the electrodes at the end of the 100 μ s pulse. Note: The color legend in subfigure c) is capped at 2 K.

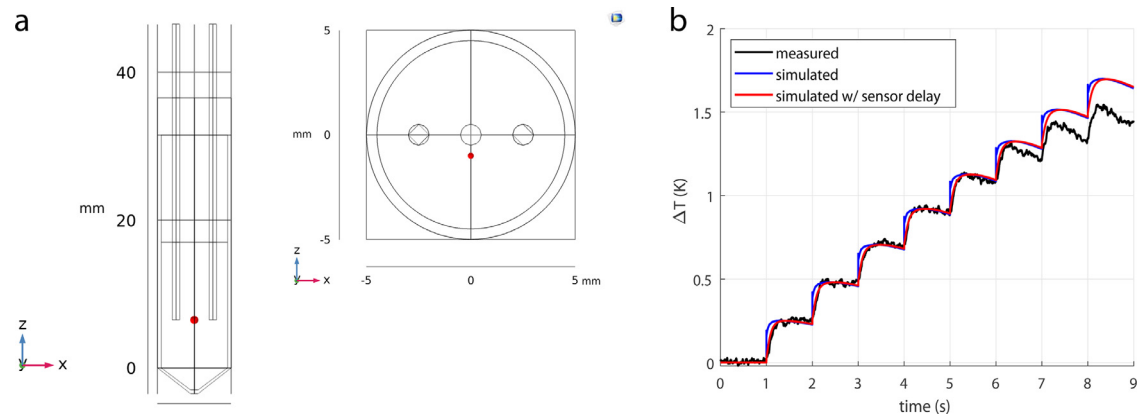


Fig. 8. Validation of the dynamic model of voltage-current relations in saline; (a) red dot indicating the approximate location of the temperature sensor tip in the experimental setup, (b) simulated temperature dynamics for one train of 8 pulses of 100 μ s delivered at 1 Hz (Protocol 8 \times 100) at the point identified in the preceding subfigure, with comparison to the experimentally measured temperature at that point. Gold (Au) electrodes were used for experiments. (For interpretation of the references to colour in this figure legend, the reader is referred to the web version of this article.)

viewed from the side of the tube. We performed several experiments using a secondary temperature probe to make sure the primary temperature gauge remained within the specified range for dynamics, resolution, and accuracy.

Fig. 8 conveys the approximate location of the temperature sensor tip as used in the experiments for model validation. We measured the temperature slightly off-center, i.e. about 1 mm from the plane in which the two electrodes lie, and equidistant to the two electrodes. From the strategic point of view the chosen location is not ideal, as the temperature gradient can be substantial at this point (see Fig. 7). It is, however, the position in which – given the chosen geometry and setup – it was easiest to achieve good repeatability of sensor positioning. Given a more elaborate measurement setup, we would have opted for a location approximately 4–5 mm higher along the z axis, i.e. somewhere right in the middle of the submerged part of the electrode lengthwise.

Although the simulated temperature does not exactly match the experimentally determined curve, the comparison must be made in light of the simplifications and assumptions we have made during model construction. Our proposed explanation is that there is an unaccounted-for effect of cooling at the point of analysis, which becomes evident after pulse 6. The point under examination is cooled either via the metal electrodes and wires, or, more likely, via some other transfer mechanism (e.g. convective flow within the tube). This additional cooling results in the temperature dropping more rapidly during pauses in between pulses, in contrast to the simulation. The apparent discrepancy in rise time during the pulse can be attributed to limited dynamic response of the sensor, which is unable to keep up with the almost instantaneous (as simulated) temperature rise. In order to incorporate the impact of sensor's finite response time, we imported the obtained temperature dynamics from COMSOL into MATLAB, where it was filtered using a first-order Butterworth filter with a cut-off frequency of 5 Hz (sensor's response time is around 200 ms). The resulting filtered curve fits the measured signal much better. See Fig. 8b to compare the measured signal (in black) to the simulated (blue line) and to the simulated and filtered with the low-pass first-order filter (red line).

To determine if the increase in current within a train of pulses is due to a rise in temperature alone via its effect on conductivity, or whether there are other contributions to be considered, we analyzed the current increase for the three protocols and compared the measurements to the predicted current increase, if we only take into account the increase in medium conductivity due to the increase in temperature. The results of analysis are collected in Table 2.

Note that in order to obtain data collected in Table 2, columns 1–2, each experiment was performed six times using the same protocol, with the two furthest outliers of the six taken excluded from the final average. Electrode surface was refurbished between every repetition of the experiment to ensure minimal impact of oxide formation, if any. The third column in Table 2, Predicted relative current increase, is the result of a calculation based on EIS (electrical impedance spectroscopy) measurements of the saline at different temperatures over a range of 10 °C in the frequency range corresponding roughly to the power spectra of the pulses (excluding the lower frequencies where polarization effects are pronounced). In other words, conductivity of the solution was carefully measured using the impedance analyzer over a range of temperatures at high frequencies, and the temperature coefficient of the solution was thus precisely determined. The temperature coefficient, given the corresponding increase in temperature by either 1.47, 1.40, or 1.93 °C, is calculated to be responsible for an increase in current as given in column 3, Table 2. The value of this coefficient is 2.15%/°C, which falls close to the temperature coefficients reported in the literature [53,63].

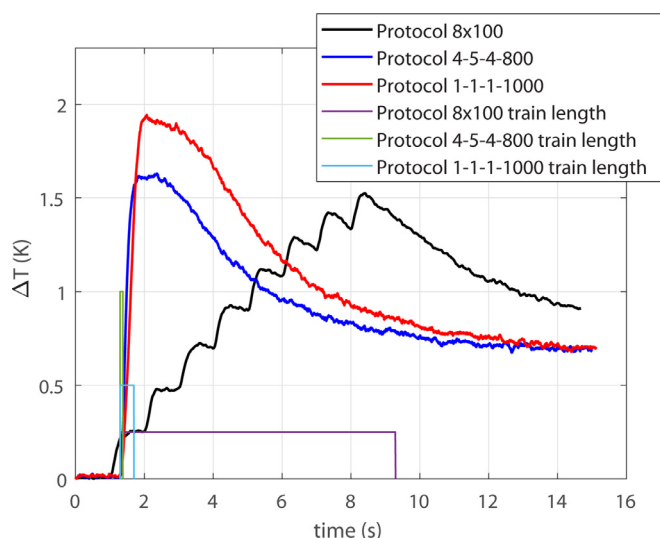


Fig. 9. Temperature profiles for the three protocols as recorded by the optical sensor immersed in saline during pulse application. Total pulse train duration is also drawn in aid of comparing and interpreting temperature dynamics. Note that train length amplitude (0.25, 0.5, and 1.0) bears no significance and was arbitrarily chosen to prevent curves from overlapping.

For all protocols we found a near perfect match between the measured increase in current from the beginning of the train of pulses to its end and the calculated or predicted current. Result is marginally better for Protocol 8×100 and Protocol 4-5-4-800, relative error is only about 1.6–1.7%, while for Protocol 1-1-1-1000, the discrepancy (error) is somewhat larger with 1.9% relative error. This can still be considered a good match, especially considering the difficult nature of controlling the position of the tip of the temperature sensor.

In order to try and understand why different protocols result in varying degrees of relative current increases during pulse application, it would be necessary to do more experimental as well as simulation studies using a different protocols and tightly controlled measurements on an improved experimental setup. A possible explanation that we can offer at this stage revolves around the duration of an individual pulse train. Given that protocols are matched to their “ON” time, we are delivering about the same energy (voltage and current are comparable, thus energy – this has been experimentally verified), but over a shorter period of time. Applying current at higher power bears the consequence that, locally, as heat will not have had the time to dissipate outside the area where it is generated, a limited volume of increased temperature mainly along the longitudinal plane in which lie both of the electrodes (the XZ-plane, refer to Fig. 7) will be formed. This area of high current density and high temperature will experience an increase in conductivity disproportionately larger as compared to the area outside of the “hot spot”, which in turn increases the current density along the already preferential current path. The process is self-sustaining and results in a more heterogeneous current density and temperature distribution, with relationship between the pulse power and the ability of the electrolyte to dissipate heat being crucial governing factors of this process. Following this rationale, it is possible to explain the difference between Protocol 8×100 and Protocol 1-1-1-1000 (also see Fig. 9), but not between Protocol 1-1-1-1000 and Protocol 4-5-4-800. The latter is five times shorter in total duration of the train of pulses as compared to the former yet exhibits a smaller overall increase in current over its total duration. The underlying phenomenon is probably more complex than described above and requires further investigation.

Fig. 9 shows temperature profiles measured roughly in the vicinity of the point indicated in Fig. 8a. The signals have been fil-

tered with a first order low-pass Butterworth filter to remove noise with amplitude of about ± 0.1 °C. The signal very clearly demonstrates the low pulse repetition frequency of the Protocol 8×100 , whereby each and every consecutive temperature increase is attributable to a particular pulse in the series of eight pulses. Difference in rise time between the two biphasic protocols is not as pronounced as it was expected (and as is evident from simulations) due to the limited response time of the temperature sensor and overall thermal inertia of the system.

Note that the *amplitude* of the temperature profile characteristic of Protocol 1-1-1-1000 is statistically significantly different from the amplitudes of temperature response of both Protocol 4-5-4-800 and Protocol 8×100 , while there is no statistically significant difference between the amplitudes of temperature profiles of Protocol 8×100 and Protocol 4-5-4-800. In all cases the T-test on 6 samples was done using $p \leq 0.05$. Simulations show this is to be expected; The Protocol 4-5-4-800 delivers all the energy in just 81.3 ms, while the corresponding time for Protocol 1-1-1-1000 is about five times that and equals 401.2 ms. These times are both too short with respect to time constants of heat transfer by conduction given the geometry of the system and sensor positioning, and thus if electric currents (and therefore power) are the same for both protocols, the almost instantaneous temperature rise will be the same in amplitude. Variability in amplitude among different measurements as shown in Fig. 9 can be attributed to sensor positioning and other variables that are imperfectly controlled. What is different both in simulation and as observed from measurements if comparing Protocol 1-1-1-1000 and Protocol 4-5-4-800 is the *dynamics* of temperature. We see a more rapid increase in temperature for Protocol 4-5-4-800 as well as an earlier onset of thermal dissipation, resulting in a more rapid decrease in temperature as compared to Protocol 1-1-1-1000.

4.3. Electrode material and impedance measurements

To analyze the impact of electrolysis and related chemical reactions at the electrode-electrolyte interface to properties of metal electrodes, we performed impedance measurements before and after delivery of each train of pulses for all three protocols. Electrochemical phenomena at the electrodes during electrode polarization and passing of faradaic current are numerous and, in some cases, extremely complex and demanding for analysis. Different metals also tend to behave differently and are susceptible to a number of processes. These processes can cause irreversible damage or alter the metal's surface properties. Treatment of such phenomena in any detail is outside the scope of any general approach. This part of the study therefore focuses only on what we can learn about changes in electrical properties of the electrodes. In other words, we have attempted to quantify the extent to which passing high-voltage, high-current electric pulses in saline alters the impedance of the electrodes made of various metals, which is an indicator of how well the electrodes will be able to subsequently conduct current if much smaller voltages are applied, such as is the case in sensing bioelectrical signals, a problem we have alluded to already in the Introduction.

Since formation of oxidative layers on the surface of electrodes is known to have an impact on their impedance [65], we measured the impedance of the electrodes before as well as after the pulse, and refurbished (by polishing) the electrode surface between consecutive measurements using ultra-fine 1500 and 2000 grit wet sandpaper. Ideally, we would have analyzed the impedance in-between the pulses to track temporal evolution of changes to the electrodes, however, due to available equipment, experimental setup, and high pulse repetition frequencies, this has proven not to be feasible. In continuation of this impedance study, we measured impedance before and after delivery of three consecutive trains of

pulses using the same protocol, and these measurements are to be contrasted with those obtained when intermittently (i.e. in between pulse deliveries) polishing the electrode surface with sandpaper. For easier presentation and comparison, we opted not to present before and after measurements separately, but calculated the ratio of post-pulse to pre-pulse impedance, which is defined as $Z = R_s + j\omega C_s$, where ω is $2\pi f$, f being the measuring frequency, R_s is the series resistance, and C_s the series capacitance as measured by the impedance analyzer using a two-electrode method and 50 mV measuring voltage amplitude. The ratio of absolute values of impedances post- to pre-pulse, r_z , is therefore a dimensionless unit of which value lower than 1 indicates that the impedance has dropped post-pulse with respect to the initial, while values greater than 1 indicate an increase in impedance with respect to the initial, i.e. that of refurbished electrodes. For intermittently polished electrodes (i.e. surface refurbished in between pulse deliveries), the experiment consisting of a single train delivery was repeated three times, so an average value of r_z is presented. Repeatability among the three takes is high, with standard deviation typically below 0.05 for frequencies below 5 kHz where electrode polarization effects are impacting the two-electrode impedance measurements, and below 0.01 above 5 kHz where the said effects are less prominent. For sequential delivery without intermittent refurbishing of electrodes, a single experiment consisting of three consecutive pulse train deliveries was performed, and ratio of impedances is calculated based on the measurement before train 1 and that after train 3. Results are graphically collected in Fig. 10.

Fig. 10 presents the results of after-pulse with respect to before-pulse delivery electrical impedance measurements that were performed in 0.9% saline for pure gold, titanium, tantalum, platinum, and alloys nitinol, platinum-iridium, and stainless steel 304, using all three protocols used in the study. Interpretation of Fig. 10 indicates that for all metals and alloys except nitinol, for which results are highly inconclusive (and seem not to indicate a clear trend), and are therefore omitted from further discussion, we were able to detect a change in impedance spectra, particularly at lower frequencies of 50 Hz to 50 kHz. In general, monophasic pulses (Protocol 8×100) affect the impedance more than biphasic pulses (Protocol 1-1-1-1000 and 4-5-4-800), an effect possibly attributable to the phenomenon of electrode corrosion/etching altering interfacial capacitance (rougher surface). Our experimental observations also corroborate the suppositions mentioned in the Materials and Methods section; we expected to find evidence of less intense electrochemical phenomena for shorter, biphasic pulses as compared to longer, monophasic ones. This was repeatedly found to be the case, judging also from bubble formation and coalescence observations, as well as differences in electrode visual appearance (change in color), i.e. appearance of an oxidized surface layer (Fig. 1).

Of all six remaining metals under consideration, nitinol having been excluded, only tantalum exhibits an increase – as opposed to a decrease – in low-frequency impedance post-pulse. This increase in tantalum electrode impedance is an effect possibly attributable to rapid formation of an oxidative layer on the surface of the electrode. It remains to be investigated whether this trend would continue with successive trains of pulses. Despite being strongly affected by monophasic pulses, change of tantalum impedance is insignificant for biphasic pulses if electrodes are refurbished, i.e. surface-polished between deliveries (see red and grey curves for tantalum in Fig. 10), as is the case with pure titanium and platinum. If refurbishing electrode surface between pulse deliveries is not an option and electrode impedance is important, of the tested metals, platinum and titanium seem most suitable for use.

These results have practical implications. They alert to an important consideration that must be given to pulse delivery and use of electrodes as contacts for electrical sensing in light of their material composition. Depending on the material of the electrodes

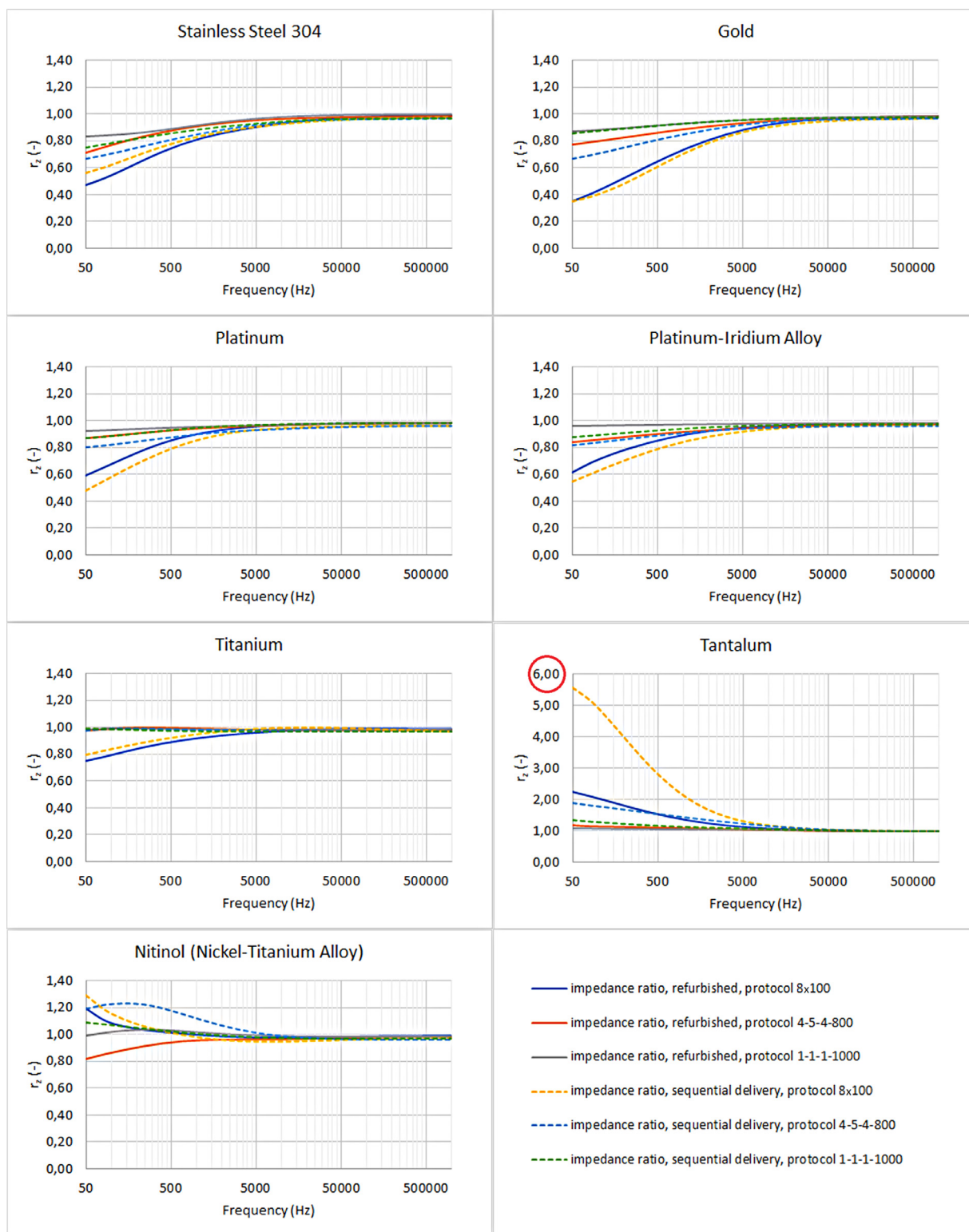


Fig. 10. Results of post- to pre-pulse two-electrode impedance measurements. Ratio r_z for seven metals/metal alloys in the frequency range of 50 Hz to 1 MHz. Note that the y axis scale for tantalum is in significantly broader range than for the other metals/alloys (denoted by the red circle). (For interpretation of the references to colour in this figure legend, the reader is referred to the web version of this article.)

(e.g. tantalum vs. stainless steel vs. titanium), and the pulse protocol, electrodes may be altered by pulse delivery such that any measuring signal originating at these same electrodes can be received attenuated, the same, or amplified as compared to before pulse delivery.

The amplification or attenuation of the signal received through post- in comparison to pre-pulse delivery electrodes is frequency dependent and affects lower frequencies more intensely than higher. The lower frequencies, for which we measured the largest difference in impedance, are also the most problematic, for two

reasons; firstly, measurements in this range are prone to error due to electrode polarization if using the two-electrode method in electrical impedance spectroscopy [66], and secondly, important biomedical signals tend to contain most significant information at lower frequencies rather than higher. For example, in intracardial ECG, the bulk of the useful signal is in the range of 30 to 100 Hz if using bipolar leads. Irrespective of whether we were able to measure accurately the absolute value of the electrode-electrolyte system impedance due to the use of the two-electrode (instead of the four-electrode) method, the results presented herein give the relative measure of post- to pre-pulse impedance, reducing any systemic error introduced by the two-electrode method that is problematic due to electrode polarization at low frequencies. It is also important to note that in routine clinical, research, and industrial applications of electroporation, any measurements of electrical or other physical properties of the treated system will involve electrodes that are also used for delivering the pulses, without the benefit of additional two electrodes reserved for measurement purposes only. In other words, changes in impedance that we were able to detect using our approach, could present a potential problem in applications of electroporation as a treatment.

The potential negative effects of electrochemistry at the electrodes are not to be taken lightly. In existing literature on clinical or industrial protocols employing electroporation, accounts containing descriptions of cleaning or refurbishing of electrodes are seldom encountered. Users of this technology must beware that although organic solvents can help with removal of organic matter from the electrodes to prevent or at least mitigate the phenomenon of electrode fouling, these solvents are unlikely to undo consequences of faradaic reactions and associated alterations of the electrodes (etching, pitting, oxidation, etc.) and restore the electrodes to their original state. We have demonstrated that if effects of pulse delivery to the electrodes must be kept at a minimum, biphasic pulses should be preferred over monophasic, and that the electrodes be regularly cleaned or replaced with new ones. Although single-use cuvettes are available, it is far more cost-effective to reuse them more than for the intended single use, a practice not to be dismissed due to numerous "instructions" on the Internet regarding "cleaning" and reusing them. Users should beware their results can be affected by not only the parameters of their treatment under their control, but also by the as yet poorly elucidated electrochemistry, associated with delivery of high-voltage, high-current pulses. As an example from clinical use; it is known in the field of electroporation applications for veterinary oncology that electrodes are at times subjected to multiple usages between treatment sessions without their surfaces being refurbished, or indeed continuously reused without any testing and control to ensure their electrical properties remain within specification. The electrode surface suitability and adherence to specifications is of utmost importance for successful delivery of pulses during electrochemotherapy or irreversible tumor ablation as these surfaces represent the conduit via which electrical energy is delivered to the target tissue. More must be done to make clinicians using electroporation in veterinary medicine aware of this, since there is considerable risk that they are more likely to reutilize the same pair of electrodes beyond manufacturer specification compared to their colleagues working with human patients.

5. Conclusions

We have set out to demonstrate the need for an in-depth look at electrochemical relations at the electrodes and electrolyte during electroporation, especially for applications where the electrochemistry might have an important impact to the treatment outcome. We have offered a detailed description of an experimental setup featuring both a well-defined geometry and a well-

characterized electrolyte for *in vitro* experimentation. This setup lends itself favorably to numerical modelling, and, provided one is capable of obtaining and recording as much information on the physical variables of the system as possible with sufficient accuracy, it is possible to obtain a good agreement between experimental observations and model simulation predictions.

Future research directions indicated point towards advanced modelling of phenomena related to metal corrosion/erosion, gas bubble formation and migration, pH changes, and the effects of acidic/alkaline medium at the electrode surface (redox reactions). Since 0.9% saline was found to be similar enough to e.g. a nutrient mixture (cell growth medium, often used as an electroporation medium) in its electrical properties, it can serve as a suitable model for the medium surrounding cells in an *in vitro* environment during electroporation. We thus propose a possibility of tackling more challenging considerations of high-voltage electrochemistry by building upon a solid framework constructed using this humble, simple indifferent fluid.

Credit author statement

The Authors declare all figures and materials incorporated into the manuscript are the Authors' own work and therefore no permission needs to be obtained from any material copyright holders.

Declaration of Competing Interest

The authors declare that they have no known competing financial interests or personal relationships that could have appeared to influence the work reported in this paper.

Acknowledgments

The work was funded through research programs and projects funded by the Slovenian Research Agency (ARRS), namely research program P2-0249 and postdoctoral project Z7-1886, and Medtronic, Inc. The work was performed within the scope of the Infrastructural Centre "Cellular Electrical Engineering" (I0-0022). SMK would like to thank Rok Šmerc from University of Ljubljana for helpful discussions about modelling and simulation in COMSOL. Both authors acknowledge the help of Gonzalo Martinez from Medtronic, Inc. in preparation of this manuscript and suggestions on improving the study and thank Angelika Vižintin and Alenka Maček Lebar from University of Ljubljana for constructive criticisms of the manuscript. Both authors acknowledge the help in improving the original manuscript based on helpful comments of reviewers upon submission to *Electrochimica Acta*.

Supplementary materials

Supplementary material associated with this article can be found, in the online version, at [doi:10.1016/j.electacta.2020.137187](https://doi.org/10.1016/j.electacta.2020.137187).

Reference

- [1] T. Kotnik, L. Rems, M. Tarek, D. Miklavčič, Membrane electroporation and electroporation: mechanisms and models, *Ann. Rev. Biophys.* 48 (2019) 63–91, doi:[10.1146/annurev-biophys-052118-115451](https://doi.org/10.1146/annurev-biophys-052118-115451).
- [2] K. Kinoshita, I. Ashikawa, N. Saita, H. Yoshimura, H. Itoh, K. Nagayama, A. Ikegami, Electroporation of cell membrane visualized under a pulsed-laser fluorescence microscope, *Biophys. J.* 53 (1988) 1015–1019.
- [3] S. Haberl, D. Miklavčič, G. Sersa, W. Frey, B. Rubinsky, Cell membrane electroporation-Part 2: the applications, *IEEE Electr. Insul. Mag.* 29 (2013) 29–37, doi:[10.1109/MEI.2013.6410537](https://doi.org/10.1109/MEI.2013.6410537).
- [4] F.J. Barba, O. Parniakov, S.A. Pereira, A. Wiktor, N. Grimi, N. Boussetta, J.A. Saraiva, J. Raso, O. Martin-Belloso, D. Witrowa-Rajchert, N. Lebovka, E. Vorobiev, Current applications and new opportunities for the use of pulsed electric fields in food science and industry, *Food Res. Int.* 77 (2015) 773–798, doi:[10.1016/j.foodres.2015.09.015](https://doi.org/10.1016/j.foodres.2015.09.015).

- [5] A. Golberg, M. Sack, J. Teissie, G. Pataro, U. Pliquett, G. Saulis, T. Stefan, D. Miklavčič, E. Vorobiev, W. Frey, Energy-efficient biomass processing with pulsed electric fields for bioeconomy and sustainable development, *Biotechnol. Biofuels* 9 (2016) 94, doi:10.1186/s13068-016-0508-z.
- [6] M.L. Yarmush, A. Golberg, G. Serša, T. Kotnik, D. Miklavčič, Electroporation-based technologies for medicine: principles, applications, and challenges, *Ann. Rev. Biomed. Eng.* 16 (2014) 295–320, doi:10.1146/annurev-bioeng-071813-104622.
- [7] G. Pataro, G. Donsi, G. Ferrari, Modeling of electrochemical reactions during pulsed electric field treatment, in: D. Miklavčič (Ed.), *Handbook of Electroporation*, Springer International Publishing, Cham, 2016, pp. 1–30, doi:10.1007/978-3-319-26779-1_5-1.
- [8] B. Roodenburg, J. Morren, H.E. (Iekje) Berg, S.W.H. de Haan, Metal release in a stainless steel Pulsed Electric Field (PEF) system: part I. Effect of different pulse shapes; theory and experimental method, *Innov. Food Sci. Emerg. Technol.* 6 (2005) 327–336, doi:10.1016/j.ifset.2005.04.006.
- [9] B. Roodenburg, J. Morren, H.E. Berg, S.W.H. de Haan, Metal release in a stainless steel pulsed electric field (PEF) system Part II. The treatment of orange juice; related to legislation and treatment chamber lifetime, *Innov. Food Sci. Emerg. Technol.* 6 (2005) 337–345, doi:10.1016/j.ifset.2005.04.004.
- [10] G. Saulis, R. Rodaitė-Risevičienė, V. Snitka, Increase of the roughness of the stainless-steel anode surface due to the exposure to high-voltage electric pulses as revealed by atomic force microscopy, *Bioelectrochemistry* 70 (2007) 519–523, doi:10.1016/j.bioelechem.2006.12.003.
- [11] G. Pataro, M. Falcone, G. Donsi, G. Ferrari, Metal release from stainless steel electrodes of a PEF treatment chamber: effects of electrical parameters and food composition, *Innov. Food Sci. Emerg. Technol.* 21 (2014) 58–65, doi:10.1016/j.ifset.2013.10.005.
- [12] G. Pataro, G.M.J. Barca, G. Donsi, G. Ferrari, On the modeling of electrochemical phenomena at the electrode-solution interface in a PEF treatment chamber: methodological approach to describe the phenomenon of metal release, *J. Food Eng.* 165 (2015) 34–44, doi:10.1016/j.jfoodeng.2015.05.009.
- [13] G. Pataro, G.M.J. Barca, G. Donsi, G. Ferrari, On the modelling of the electrochemical phenomena at the electrode-solution interface of a PEF treatment chamber: effect of electrical parameters and chemical composition of model liquid food, *J. Food Eng.* 165 (2015) 45–51, doi:10.1016/j.jfoodeng.2015.05.010.
- [14] J. Morren, B. Roodenburg, S.W.H. de Haan, Electrochemical reactions and electrode corrosion in pulsed electric field (PEF) treatment chambers, *Innov. Food Sci. Emerg. Technol.* 4 (2003) 285–295, doi:10.1016/S1466-8564(03)00041-9.
- [15] N. Meneses, H. Jaeger, D. Knorr, pH-changes during pulsed electric field treatments – Numerical simulation and in situ impact on polyphenoloxidase inactivation, *Innov. Food Sci. Emerg. Technol.* 12 (2011) 499–504, doi:10.1016/j.ifset.2011.07.001.
- [16] M. Kim, H.Q. Zhang, Improving electrode durability of PEF chamber by selecting suitable material, in: *Nonthermal Processing Technologies For Food*, John Wiley & Sons, Ltd, 2011, pp. 201–212, doi:10.1002/9780470958360.ch14.
- [17] L. Lambricht, A. Lopes, S. Kos, G. Sersa, V. Prêat, G. Vandermeulen, Clinical potential of electroporation for gene therapy and DNA vaccine delivery, *Expert Opin Drug Deliv.* 13 (2016) 295–310, doi:10.1517/17425247.2016.1121990.
- [18] L.G. Campana, I. Edhemovic, D. Soden, A.M. Perrone, M. Scarpa, L. Campanacci, M. Cemazar, S. Valpione, D. Miklavčič, S. Mocellin, E. Sieni, G. Sersa, Electrochemotherapy – Emerging applications technical advances, new indications, combined approaches, and multi-institutional collaboration, *Eur. J. Surg. Oncol.* 45 (2019) 92–102, doi:10.1016/j.ejso.2018.11.023.
- [19] H.J. Scheffer, K. Nielsen, M.C. de Jong, A.A.J.M. van Tilborg, J.M. Vieveen, A.R.A. Bouwman, S. Meijer, C. van Kuijk, P.M.P. van den Tol, M.R. Meijerink, Irreversible electroporation for nonthermal tumor ablation in the clinical setting: a systematic review of safety and efficacy, *J. Vasc. Interv. Radiol.* 25 (2014) 997–1011 quiz 1011, doi:10.1016/j.jvir.2014.01.028.
- [20] E. Maor, A. Sugrue, C. Witt, V.R. Vaidya, C.V. DeSimone, S.J. Asirvatham, S. Kapa, Pulsed electric fields for cardiac ablation and beyond: a state-of-the-art review, *Heart Rhythm* 16 (2019) 1112–1120, doi:10.1016/j.hrthm.2019.01.012.
- [21] A. Sugrue, V. Vaidya, C. Witt, C.V. DeSimone, O. Yasin, E. Maor, A.M. Killu, S. Kapa, C.J. McLeod, D. Miklavčič, S.J. Asirvatham, Irreversible electroporation for catheter-based cardiac ablation: a systematic review of the preclinical experience, *J. Interv. Card. Electrophysiol.* 55 (2019) 251–265, doi:10.1007/s10840-019-00574-3.
- [22] V.Y. Reddy, P. Neuzil, J.S. Koruth, J. Petru, M. Funosako, H. Cochet, L. Sediva, M. Chovanec, S.R. Dukkipati, P. Jais, Pulsed field ablation for pulmonary vein isolation in atrial fibrillation, *J. Am. Coll. Cardiol.* 74 (2019) 315–326, doi:10.1016/j.jacc.2019.04.021.
- [23] M.T. Stewart, D.E. Haines, A. Verma, N. Kirchhof, N. Barka, E. Grassl, B. Howard, Intracardiac pulsed field ablation: proof of feasibility in a chronic porcine model, *Heart Rhythm* 16 (2019) 754–764, doi:10.1016/j.hrthm.2018.10.030.
- [24] A. Wojtaszczyk, G. Caluori, M. Pešl, K. Melajova, Z. Stárek, Irreversible electroporation ablation for atrial fibrillation, *J. Cardiovasc. Electrophysiol.* 29 (2018) 643–651, doi:10.1111/jce.13454.
- [25] J.S. Koruth, K. Kuroki, J. Iwasawa, R. Viswanathan, R. Brose, E.D. Buck, E. Don-skoy, S.R. Dukkipati, V.Y. Reddy, Endocardial ventricular pulsed field ablation: a proof-of-concept preclinical evaluation, *Europace* 22 (2020) 434–439, doi:10.1093/europace/euz341.
- [26] F.H.M. Wittkamp, R. van Es, K. Neven, Electroporation and its relevance for cardiac catheter ablation, *J. Am. Coll. Cardiol. EP* 4 (2018) 977–986, doi:10.1016/j.jacep.2018.06.005.
- [27] K. Bor, D. Miklavčič, Numerical modelling of the influence of tissue-electrode contact during cardiac ablation by IRE, in: *Programme and Book of Abstracts of the 3rd World Congress on Electroporation and Pulsed Electric Fields in Biology, Medicine, and Food & Environmental Technologies, ISEBTT - The International Society for Electroporation-Based Technologies and Treatments, Toulouse, France, 2019*, p. 176.
- [28] J.M. Demolin, O.J. Eick, K. Münch, E. Koullick, H. Nakagawa, F.H.M. Wittkamp, Soft thrombus formation in radiofrequency catheter ablation, *Pacing Clin. Electrophysiol.* 25 (2002) 1219–1222, doi:10.1046/j.1460-9592.2002.01219.x.
- [29] E. Nagy-Baló, D. Tint, M. Clemens, I. Beke, K.R. Kovács, L. Csiba, I. Édes, Z. Csanádi, Transcranial measurement of cerebral microembolic signals during pulmonary vein isolation: a comparison of two ablation techniques, *Circ. Arrhythm Electrophysiol.* 6 (2013) 473–480, doi:10.1161/CIRCEP.112.971747.
- [30] A. Kiss, E. Nagy-Baló, G. Sándorfi, I. Édes, Z. Csanádi, Cerebral microembolization during atrial fibrillation ablation: comparison of different single-shot ablation techniques, *Int. J. Cardiol.* 174 (2014) 276–281, doi:10.1016/j.ijcard.2014.03.175.
- [31] E. Nagy-Baló, A. Kiss, C. Condie, M. Stewart, I. Édes, Z. Csanádi, Predictors of cerebral microembolization during phased radiofrequency ablation of atrial fibrillation: analysis of biophysical parameters from the ablation generator, *Heart Rhythm* 11 (2014) 977–983, doi:10.1016/j.hrthm.2014.03.018.
- [32] M. Takami, H.I. Lehmann, K.D. Parker, K.M. Welker, S.B. Johnson, D.L. Packer, Effect of left atrial ablation process and strategy on microemboli formation during irrigated radiofrequency catheter ablation in an in vivo model, *Circ. Arrhythm Electrophysiol.* 9 (2016) e003226, doi:10.1161/CIRCEP.115.003226.
- [33] D.E. Haines, M.T. Stewart, S. Dahlberg, N.D. Barka, C. Condie, G.R. Fiedler, N.A. Kirchhof, F. Halimi, T. Deneke, Microembolism and catheter ablation I: a comparison of irrigated radiofrequency and multielectrode-phased radiofrequency catheter ablation of pulmonary vein ostia, *Circ. Arrhythm. Electrophysiol.* 6 (2013) 16–22, doi:10.1161/CIRCEP.111.973453.
- [34] A. Verma, P. Debruyne, S. Nardi, T. Deneke, Y. DeGreef, S. Spitzer, J.O. Balzer, L. Boersma, ERACE Investigators, Evaluation and reduction of asymptomatic cerebral embolism in ablation of atrial fibrillation, but high prevalence of chronic silent infarction: results of the evaluation of reduction of asymptomatic cerebral embolism trial, *Circ. Arrhythm. Electrophysiol.* 6 (2013) 835–842, doi:10.1161/CIRCEP.113.000612.
- [35] E. Society (U.S.), F.A. Lowenheim, *Modern Electroplating*, 3rd ed, Wiley, New York [N.Y.], 1974 <https://trove.nla.gov.au/version/45216597> (accessed December 18, 2019).
- [36] J.C. Weaver, K.C. Smith, A.T. Esser, R.S. Son, T.R. Gowrishankar, A brief overview of electroporation pulse strength-duration space: a region where additional intracellular effects are expected, *Bioelectrochemistry* 87 (2012) 236–243, doi:10.1016/j.bioelechem.2012.02.007.
- [37] L. Onsager, S.K. Kim, Wien effect in simple strong electrolytes, *J. Phys. Chem.* 61 (1957) 198–215, doi:10.1021/j150548a015.
- [38] M. Pavlin, M. Kanduser, M. Rebersek, G. Pucihar, F.X. Hart, R. Magjarevic, D. Miklavčič, Effect of cell electroporation on the conductivity of a cell suspension, *Biophys. J.* 88 (2005) 4378–4390, doi:10.1529/biophysj.104.048975.
- [39] M. Pavlin, D. Miklavčič, Theoretical and experimental analysis of conductivity, ion diffusion and molecular transport during cell electroporation—Relation between short-lived and long-lived pores, *Bioelectrochemistry* 74 (2008) 38–46, doi:10.1016/j.bioelechem.2008.04.016.
- [40] M. Kranjc, F. Bajd, I. Serša, D. Miklavčič, Magnetic resonance electrical impedance tomography for measuring electrical conductivity during electroporation, *Physiol. Meas.* 35 (2014) 985–996, doi:10.1088/0967-3334/35/6/985.
- [41] J. Blahovec, E. Vorobiev, N. Lebovka, Pulsed electric fields pretreatments for the cooking of foods, *Food Eng. Rev.* 9 (2017) 71–81, doi:10.1007/s12393-017-9160-z.
- [42] IXL – e-Cooking Technology, (n.d.). <http://www.e-cooking-technology.com/> (accessed December 18, 2019).
- [43] N. Olaiz, E. Signori, F. Maglietti, A. Soba, C. Suárez, P. Turjanski, S. Michinski, G. Marshall, Tissue damage modeling in gene electrotransfer: the role of pH, *Bioelectrochemistry* 100 (2014) 105–111, doi:10.1016/j.bioelechem.2014.05.001.
- [44] M. Phillips, L. Rubinsky, A. Meir, N. Raju, B. Rubinsky, Combining electrolysis and electroporation for tissue ablation, *Technol. Cancer Res. Treat.* (2014), doi:10.1177/1533034614560102.
- [45] N. Klein, E. Guenther, F. Botea, M. Pautov, S. Dima, D. Tomescu, M. Popescu, A. Ivorra, M. Stehling, I. Popescu, The combination of electroporation and electrolysis (E2) employing different electrode arrays for ablation of large tissue volumes, *PLoS One* 14 (2019), doi:10.1371/journal.pone.0221393.
- [46] E. Luján, M. Marino, N. Olaiz, G. Marshall, Towards an optimal dose-response relationship in gene electrotransfer protocols, *Electrochim. Acta* 319 (2019) 1002–1011, doi:10.1016/j.electacta.2019.07.029.
- [47] N. Klein, B. Mercadal, M. Stehling, A. Ivorra, *in vitro* study on the mechanisms of action of electrolytic electroporation (E2), *Bioelectrochemistry* 133 (2020), doi:10.1016/j.bioelechem.2020.107482.
- [48] K.S. Gates, An overview of chemical processes that damage cellular dna: spontaneous hydrolysis, alkylation, and reactions with radicals, *Chem. Res. Toxicol.* 22 (2009) 1747–1760, doi:10.1021/tx900242k.
- [49] M. Ageno, E. Dore, C. Frontali, The alkaline denaturation of DNA, *Biophys. J.* 9 (1969) 1281–1311.
- [50] T.E. Creighton, *The Biophysical Chemistry of Nucleic Acids and Proteins*, Helvetic Press, Eastbourne, East Sussex, 2010.
- [51] I. Lacković, R. Magjarević, D. Miklavčič, Three-dimensional finite-element analysis of joule heating in electrochemotherapy and *in vivo* gene electrotransfer, *IEEE Trans. Dielectr. Electr. Insul.* 16 (2009) 1338–1347, doi:10.1109/TDEI.2009.5293947.
- [52] A.S. Quist, W.L. Marshall, Electrical conductances of aqueous sodium chloride

- solutions from 0 to 800.degree. and at pressures to 4000 bars, *J. Phys. Chem.* 72 (1968) 684–703, doi:10.1021/j100848a050.
- [53] C.G. Malmberg, *Electrical conductivity of dilute solutions of " Sea Water " From 5 to 120 °C*, *J. Res. Natl. Bureau of Stand.- A. Phys. Chem.* 69A (1965) 39–43.
- [54] N. Boc, I. Edhemovic, B. Kos, M.M. Music, E. Breclj, B. Trotovsek, M. Bosnjak, M. Djokic, D. Miklavcic, M. Cemazar, G. Sersa, Ultrasonographic changes in the liver tumors as indicators of adequate tumor coverage with electric field for effective electrochemotherapy, *Radiol. Oncol* 52 (2018) 383–391, doi:10.2478/raon-2018-0041.
- [55] H. Li, S. Sun, J.Q. Yap, J. Chen, Q. Qian, 0.9% saline is neither normal nor physiological, *J. Zhejiang Univ. Sci. B* 17 (2016) 181–187, doi:10.1631/jzus.B1500201.
- [56] E.L. Latouche, C.B. Arena, J.W. Ivey, P.A. Garcia, T.E. Pancotto, N. Pavlisko, S.S. Verbridge, R.V. Davalos, J.H. Rossmeisl, High-frequency irreversible electroporation for intracranial meningioma: a feasibility study in a spontaneous canine tumor model, *Technol. Cancer Res. Treat.* 17 (2018), doi:10.1177/1533033818785285.
- [57] C.B. Arena, M.B. Sano, J.H. Rossmeisl, J.L. Caldwell, P.A. Garcia, M.N. Rylander, R.V. Davalos, High-frequency irreversible electroporation (H-FIRE) for non-thermal ablation without muscle contraction, *Biomed. Eng. Online* 10 (2011) 102, doi:10.1186/1475-925X-10-102.
- [58] D. Miklavčič, G. Pucihar, M. Pavlovec, Š. Ribarič, M. Mali, A. Maček-Lebar, M. Petkovšek, J. Nastran, S. Kranjc, M. Čemažar, G. Serša, The effect of high frequency electric pulses on muscle contractions and antitumor efficiency *in vivo* for a potential use in clinical electrochemotherapy, *Bioelectrochemistry* 65 (2005) 121–128, doi:10.1016/j.bioelechem.2004.07.004.
- [59] J. Gehl, G. Sersa, L.W. Matthiessen, T. Muir, D. Soden, A. Occhini, P. Quaglino, P. Curatolo, L.G. Campana, C. Kunte, A.J.P. Clover, G. Bertino, V. Farricha, J. Odili, K. Dahlstrom, M. Benazzo, L.M. Mir, Updated standard operating procedures for electrochemotherapy of cutaneous tumours and skin metastases, *Acta Oncol* 57 (2018) 874–882, doi:10.1080/0284186X.2018.1454602.
- [60] D.C. Sweeney, M. Reberšek, J. Dermol, L. Rems, D. Miklavčič, R.V. Davalos, Quantification of cell membrane permeability induced by monopolar and high-frequency bipolar bursts of electrical pulses, *Biochimica et Biophysica Acta (BBA) - Biomembranes* 1858 (2016) 2689–2698, doi:10.1016/j.bbamem.2016.06.024.
- [61] Which Current Distribution Interface Do I Use?, COMSOL Multiphysics. (n.d.). <https://www.comsol.com/blogs/current-distribution-interface-use/> (accessed December 20, 2019).
- [62] Theory of Current Distribution, COMSOL Multiphysics. (n.d.). <https://www.comsol.com/blogs/theory-current-distribution/> (accessed December 20, 2019).
- [63] Martin B. Kraichman, The resistivity of aqueous solutions of sodium chloride. NOLTR 64-42, United States Naval Ordnance Laboratory, White Oak, Maryland, March 1964. <https://apps.dtic.mil/dtic/tr/fulltext/u2/437890.pdf> (accessed December 20, 2019).
- [64] W.M. Haynes, *CRC Handbook of Chemistry and Physics*, 93rd edition, CRC Press, 2012.
- [65] M. Grdeň, Impedance study on the capacitance of silver electrode oxidised in alkaline electrolyte, *J. Solid State Electrochem.* 21 (2017) 3333–3344, doi:10.1007/s10008-017-3684-2.
- [66] P. Mirtaheeri, S. Grimnes, G. Martinsen, Electrode polarization impedance in weak NaCl aqueous solutions, *IEEE Trans. Biomed. Eng.* 52 (2005) 2093–2099, doi:10.1109/TBME.2005.857639.